Available online at www.sciencedirect.com
SCIENCE DIRECT®
Journal of Solid State Chemistry 173 (2003) 91–100
JOURNAL OF SOLID STATE CHEMISTRY
http://elsevier.com/locate/jssc

HRTEM study of cation-deficient perovskite-related $A_nB_{n-\delta}O_{3n}$ ($n \geqslant 4\delta$) microphases in the $Ba_5Nb_4O_{15}$–$BaTiO_3$ system

G. Trolliard,* N. Ténèze, Ph. Boullay, M. Manier, and D. Mercurio

Science des Procédés Céramiques et de Traitements de Surface, Faculté des Sciences et Techniques, UMR-CNRS 6638, 123 avenue Albert Thomas, 87060 Limoges Cedex, France

Received 17 October 2002; received in revised form 14 January 2003; accepted 18 January 2003

Abstract

The occurrence of coherent intergrowths of cation-deficient perovskites in the $Ba_5Nb_4O_{15}$–$BaTiO_3$ system has been examined by high-resolution transmission electron microscopy and selected area electron diffraction. Because of their structural similarity, the simple members $Ba_5Nb_4O_{15}$ ($n = 5$) and $Ba_6TiNb_4O_{18}$ ($n = 6$) form coherent intergrowths—noted 5^P6^1—by the juxtaposition along the c-axis of P perovskite-like blocks $n = 5$ and one perovskite-like block $n = 6$, with $P = 1$, 2 and 3. More generally, the ability to form intergrowths in the hexagonal perovskite systems is discussed considering the structural characteristics of the simple members. Examples taken from various systems show that the formation of such intergrowths is highly dependent on the size of the A cation present in simple members.

Keywords: Cation-deficient perovskite; Intergrowths; Electron diffraction; HRTEM

1. Introduction

Among the perovskite-related structures, the "hexagonal" perovskites differ from the "ideal" cubic stacking of the perovskite by the existence of mixed cubic-hexagonal AO_3 stacking sequences. They can be described using the Jagodzinski notation [1,2] where a layer in the sequence is denoted h or c dependent upon whether its neighboring layers are alike or different. B-site vacancies are often encountered (see [3] for general structural information) and, in case of (hhc…c)-type sequences, are usually localized between the hh layers resulting in a completely vacant octahedral layer. These structures, with the general formulation $A_nB_{n-1}O_{3n}$, possess only blocks of $n-1$ corner-sharing octahedra separated by vacant octahedral layers. These oxides which form a series of trigonal structures are observed in various systems [4–20]: $A = Ba^{2+}$, Ca^{2+}, Sr^{2+}, La^{3+}, $B = Mg^{2+}$, Zn^{2+}, Al^{3+}, Ti^{3+}, Nb^{4+}, Ru^{4+}, Ti^{4+}, Nb^{5+}, Ta^{5+}.

Based on simple members n and $(n+1)$, complex intergrowths with more or less long periodicity can be formed as illustrated for instance in the system $La_4Ti_3O_{12}$–$LaTiO_3$ [21,22]. In this system it was shown that when these complex intergrowths are ordered, they are based on uniform sequences and can be described using the superspace group approach [23]. This behavior is a general trend that was observed in some other closely related systems and recently in the $La_4Ti_3O_{12}$–$BaTiO_3$ system [24].

While the crystal structure analyses of such intergrowths are now well documented [23,25], the origin of the relative stability of the various uniform sequences within a given system is still unclear. In our recent transmission electron microscopy (TEM) investigation of the $La_4Ti_3O_{12}$–$BaTiO_3$ system, we have identified, in the $La_4Ti_3O_{12}$ rich-part of the phase diagram, the existence of complex intergrowths [26,27] based on uniform sequences between perovskite blocks of the type $n = 4$ ($La_4Ti_3O_{12}$) and $n = 5$ ($BaLa_4Ti_4O_{15}$). On the contrary, no intergrowth terms were observed for compositions ranging from $BaLa_4Ti_4O_{15}$ ($n = 5$) to $Ba_2La_4Ti_5O_{18}$ ($n = 6$). In Ref. [27], we suggested that the intergrowth stability seems to be highly sensitive

*Corresponding author. Fax: +33-5-55-45-72-70.
E-mail address: trolliard@unilim.fr (G. Trolliard).

0022-4596/03/$ - see front matter © 2003 Elsevier Science (USA). All rights reserved.
doi:10.1016/S0022-4596(03)00097-5

to the difference in average size of the A cation ($r_{La3+} < r_{Ba2+}$) between the n and $n+1$ simple terms. In order to confirm this assumption, we decided to investigate the related system $Ba_5Nb_4O_{15}$–$BaTiO_3$ in which both $n = 5$ ($Ba_5Nb_4O_{15}$) and $n = 6$ ($Ba_6Nb_4TiO_{18}$) compounds are known [18,19] and have the same A cation, which seems a favorable case for testing the formation of intergrowths. Also in this system, a previous study performed by X-ray diffraction on several samples with compositions ranging from $n = 5$ to 6 [28] has revealed typical peak shifts, as a function of the composition, that can be attributed to the existence of intergrowths [27].

The first part of this paper is devoted to the description and the comparison of the crystal structures of $Ba_5Nb_4O_{15}$ ($n = 5$) and $Ba_6TiNb_4O_{18}$ ($n = 6$) where it will be shown that the structural similarities between the two compounds is a favorable case for the formation of intergrowths. In the second part, the various ordered intergrowths (usually called microphases) observed will be presented based on an extensive TEM study. Lastly, the results will be discussed and compared with the observations made in related systems and notably with our previous study of the $La_4Ti_3O_{12}$–$BaTiO_3$ system.

2. Experimental

Seven intergrowth compositions were synthesized (Table 1). All these samples were prepared as white or light yellow colored powders by conventional solid state synthesis, using high purity $BaCO_3$, TiO_2 and Nb_2O_5. Five 5^P6^1 intergrowth compositions were chosen corresponding to a molar ratio $n = 5/n = 6$ ranging from $\frac{1}{1}$ to $\frac{5}{1}$. The starting materials were mixed in stoichiometric proportions in an agate mortar and fired at 1400–1500°C in a platinum crucible, for 15–20 h, under ambient atmosphere.

Selected area electron diffraction (SAED) patterns and high-resolution transmission electron microscopy (HRTEM) images were obtained with a Jeol 2010 microscope operating at 200 kV. The powder was first crushed in an agate mortar and then a drop of a suspension of powder and water was deposited and dried on a copper grid coated with a thin film of amorphous carbon. The simulated images were computed using the NCEMSS software [29] with a spherical aberration constant of 1 mm, focus spread of 10 nm, and objective aperture diameter of 3.75 nm^{-1}.

3. Structural considerations

3.1. The members n=5 ($Ba_5Nb_4O_{15}$) and n=6 ($Ba_6TiNb_4O_{18}$)

The main crystallographic parameters of these phases are reported in Table 2 [18,19]. As for most compounds of the homologous series $A_nB_{n-1}O_{3n}$, the crystal structure of these two members consists of a framework

Table 2
Main structural characteristics of $Ba_5Nb_4O_{15}$ [18] and $Ba_6TiNb_4O_{18}$ [19]

Compound	Bravais system	Space group	Cell parameters
$Ba_5Nb_4O_{15}$ ($n = 5$)	P	P-3m1	$a = 5.7883(3)$ $c = 11.7782(7)$
$Ba_6TiNb_4O_{18}$ ($n = 6$)	R	R-3m	$a = 5.7852(1)$ $c = 42.4886(3)$

Table 1
Chemical compositions and expected intergrowths in the $Ba_5Nb_4O_{15}$–$BaTiO_3$ system

	Chemical composition synthesized	$Ba_5Nb_4O_{15}$ ($n = 5$) P mol	$Ba_6TiNb_4O_{18}$ ($n = 6$) Q mol	Expected intergrowth 5^P6^Q	Bravais system	Observed intergrowth
	$Ba_{31}TiNb_{24}O_{93}$	5	1	5^56^1	R	Mixture of $5^16^1$and 5^26^1 microphases and $n = 5$ crystals
5^P6^1 terms	$Ba_{26}TiNb_{20}O_{78}$	4	1	5^46^1	R	Mixture of $5^16^1$and 5^26^1 microphases and $n = 5$ crystals
	$Ba_{21}TiNb_{16}O_{63}$	3	1	5^36^1	R	5^36^1
	$Ba_{16}TiNb_{12}O_{48}$	2	1	5^26^1	R	5^26^1
5^16^1 term	$Ba_{11}TiNb_8O_{33}$	1	1	5^16^1	R	5^16^1
5^16^Q terms	$Ba_{17}Ti_2Nb_8O_{51}$	1	2	5^16^2	R	Mixture of $5^16^1$and 5^26^1 microphases and $n = 6$ crystals
	$Ba_{23}Ti_3Nb_8O_{69}$	1	3	5^16^3	P	Mixture of $5^16^1$and 5^26^1 microphases and $n = 6$ crystals

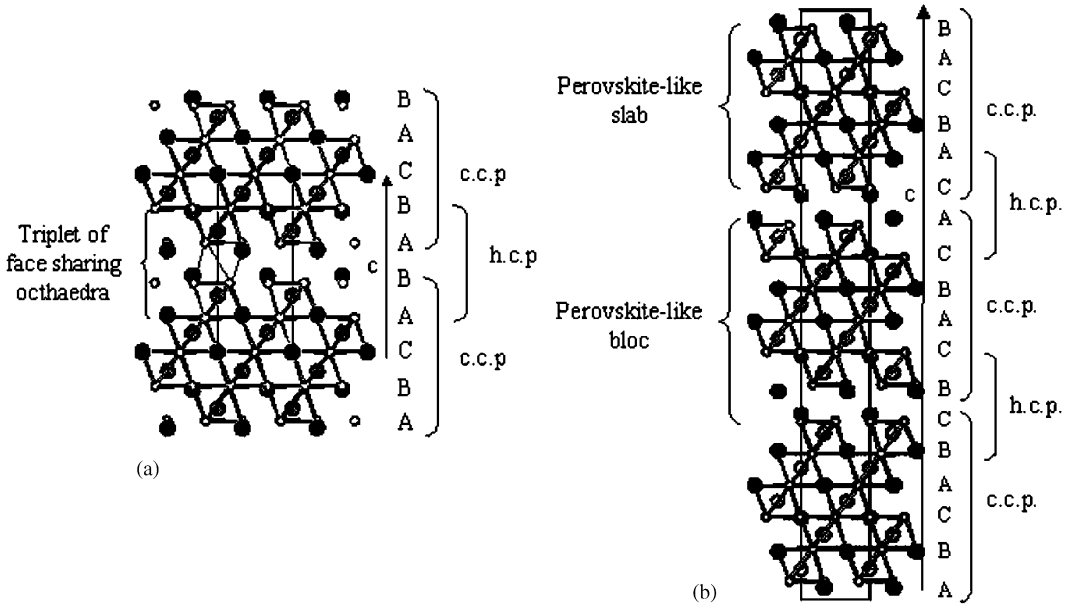

Fig. 1. Schematic representation of (a) $Ba_5Nb_4O_{15}$ ($n = 5$) and (b) $Ba_6TiNb_4O_{18}$ ($n = 6$) structures as viewed along the a-axis.

of close-packed AO_3 layers, 5H (hhccc) and 18R $(hhcccc)_3$, respectively for $n = 5$ and 6. These complex stackings give rise to mixed cubic close-packed (ccp) and hexagonal close-packed (hcp) sequences as seen in Fig. 1. The hcp part appears alike in both cases and corresponds to a triplet of face-sharing octahedra (FSO). The central octahedron of this triplet is not occupied, resulting in both cases in the formation of periodic vacant octahedral layers. In the following, we will refer to the ccp part of the structure formed by $(n-1)$ corner-sharing $(Ti,Nb)O_6$ octahedra (CSO) layer as the "perovskite-like slab". The basic sequence along the c direction formed by a perovskite-like slab and a vacant octahedra layer will be further referred as a "perovskite-like block".

As both $Ba_5Nb_4O_{15}$ and $Ba_6TiNb_4O_{18}$ contain the same A cation (barium) the AO_3 layers are alike in both structures as seen in Fig. 2 which shows the $[0001]_H$ projection of the BaO_3 layer that forms the hcp part of $Ba_5Nb_4O_{15}$ (Fig. 2a) and $Ba_6TiNb_4O_{18}$ (Fig. 2b). When superimposed, the correspondence between the atomic positions is excellent (Fig. 2c) and the interface between two perovskite-like blocks appears very similar in $n = 5$ and 6. So, the $Ba_5Nb_4O_{15}$–$BaTiO_3$ system offers a good opportunity to synthesize stable microphases between the $n = 5$ and 6 compounds (Fig. 2d).

As previously shown in the $La_4Ti_3O_{12}$–$BaTiO_3$ system [17], the TEM techniques offer a valuable help to identify the basic compounds and intergrowths. The number of close packed layers in the perovskite-like blocks and thus the periodicity of the compounds can be easily identified either by HRTEM images or SAED patterns. For both $Ba_5Nb_4O_{15}$ and $Ba_6TiNb_4O_{18}$ (Fig. 3), along the c^* direction of the SAED patterns, the first bright spot encountered from the transmitted beam (origin) corresponds to the thickness of an octahedral sheet (≈ 2.2 Å), and then the number of spots counted from the origin to this spot gives the number n of AO_3 layers in a perovskite-like block. Likewise within HRTEM images, the vacant octahedra layer always provides a specific contrast (see arrows in Fig. 3) which allows to establish the width of the perovskite-like blocks.

In order to properly associate the contrast within the HRTEM images to structural characteristics, extensive image simulations based on the crystal structure established by Pagola et al. [20] were carried out for $Ba_5Nb_4O_{15}$. Fig. 4 displays two images obtained on the same crystal for different values of focal adjustment corresponding either to slightly over-focussed condition (Fig. 4b: dark Fresnel fringes) or to under-focussed condition near the Scherzer value (Fig. 4a: bright Fresnel fringes). Simulated images superimposed onto the experimental ones are in perfect agreement with experimental conditions (sample thickness estimated to 19 nm). The examination of the projected potential map and the image calculated for a defocus value close to 45 nm (displayed together in Fig. 4c) suggests that for this condition the bright dots observed in the experimental HRTEM images can be associated with the position of the Ba atomic columns.

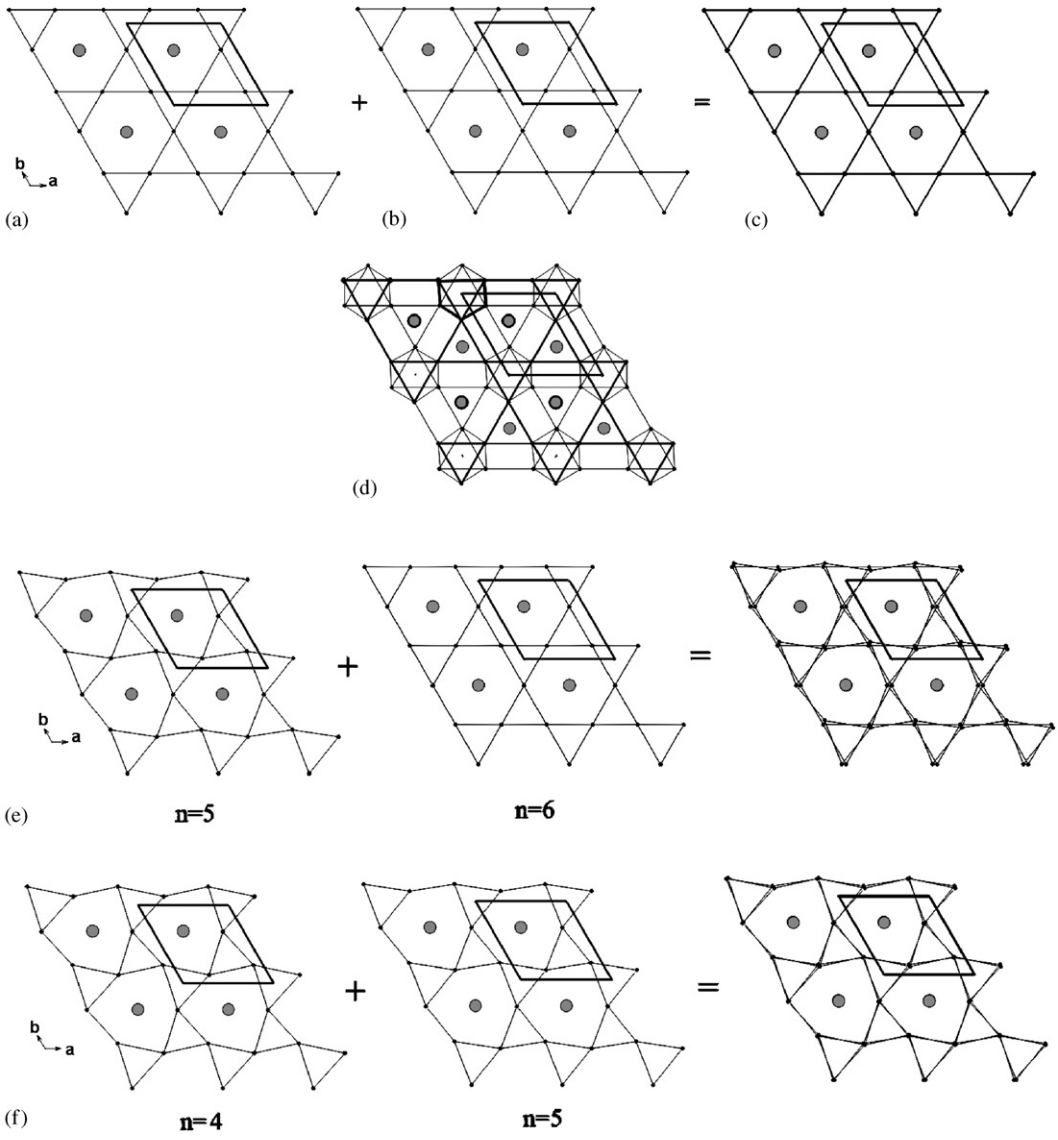

Fig. 2. $[0001]_H$ projections of the AO_3 layers of the hcp part. (a) Of $Ba_5Nb_4O_{15}$ ($n = 5$), (b) of $Ba_6TiNb_4O_{18}$ ($n = 6$), (c) superimposition of (a) and (b), (d) in-plane visualization of the interface between two different perovskite-like slab of $Ba_5Nb_4O_{15}$ and $Ba_6TiNb_4O_{18}$, built up on two successive BaO_3 layers that form the hcp part of these two compounds, (e) of $BaLa_4Ti_4O_{15}$ ($n = 5$), $Ba_2La_4Ti_5O_{18}$ ($n = 6$) and their superimposition, (f) of $La_4Ti_3O_{12}$ ($n = 4$), $BaLa_4Ti_4O_{15}$ ($n = 5$), and their superimposition.

3.2. The $Ba_n(Ti, Nb)_{n-\delta}O_{3n}$ microphases

One expects that the microphases with the composition $Ba_n(Ti,Nb)_{n-\delta}O_{3n}$ consist of the intergrowth of P perovskite-like blocks of composition $Ba_5Nb_4O_{15}$ ($n = 5$) and Q perovskite-like blocks of composition $Ba_6TiNb_4O_{18}$ ($n = 6$). The resulting chemical composition can be formulated as $P \times Ba_5Nb_4O_{15}$ ($n = 5$) + $Q \times Ba_6TiNb_4O_{18}$ ($n = 6$) and the corresponding microphases can be noted as 5^P6^Q in a compact form.

ABCAB/ABCAB/ABCABC/BCABC/BCABC/
5 5 6 5 5
BCABCA/CABCA/CABCA/CABCAB/A
6 5 5 6 .

A detailed examination of the BaO_3 layer stacking sequences leads to the following considerations:

(i) For all the 5^P6^1 intergrowths, the stacking has a repeat period which contain three 5^P6^1 blocks and thus the Bravais system is rhombohedral. As an example for the 5^26^1 microphase, the stacking sequence is:

(ii) For the 5^16^Q intergrowths, two situations have to be considered.

- If Q is a multiple of three, the stacking has a repeat period which contains a single 5^16^Q block and the Bravais system is P. For example, 5^16^3 exhibits the following sequence:

ABCAB/ABCABC/BCABCA/CABCAB/A
5 6 6 6 .

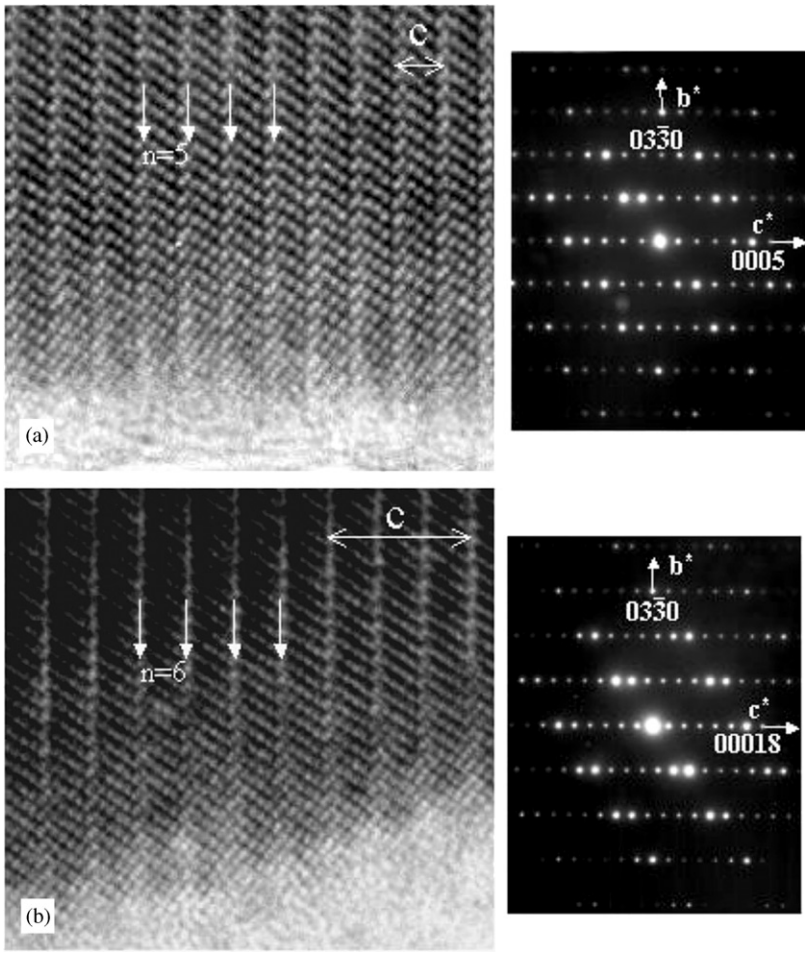

Fig. 3. TEM observations along the $[2\bar{1}\bar{1}0]_H$ zone axis. (a) Of $Ba_5Nb_4O_{15}$ ($n = 5$), (b) of $Ba_6TiNb_4O_{18}$ ($n = 6$).

- In all other cases, three 5^16^Q blocks are necessary to establish the periodicity and the Bravais system is *R*. For example, the 5^16^2 microphase is of this type, with the following stacking sequence:

$$\underset{5}{ABCAB}/\underset{6}{ABCABC}/\underset{6}{BCABCA}/\underset{5}{CABCA}/\underset{6}{CABCAB}/$$
$$\underset{6}{ABCABC}/\underset{5}{BCABC}/\underset{6}{BCABCA}/\underset{6}{CABCAB}/\underset{}{A}.$$

4. Results and discussion

For the seven synthesized powders (Table 1) and whatever the heating treatment (see experimental), intergrowth terms are always formed.

In samples submitted to an annealing treatment of 15 h at 1400°C (Fig. 5) stacking faults are frequently observed within crystals. As an example, Fig. 5 reveals abnormal 5^26^1 stacking sequences in a crystal with an initial composition corresponding to $Ba_{11}TiNb_8O_{33}$ (5^16^1 intergrowth). Accordingly, in the SAED patterns obtained for this crystal, the superstructure reflections show diffuse streaks along the c^* direction. Moreover, the diffraction patterns are apparently incommensurate with characteristic spacing anomaly (Fig. 5d). In this diagram, the spot corresponding to the average thickness of a perovskite block (Fig. 5d), which also represents the average periodicity of the distribution of vacant octahedra layers, is slightly shifted from its ideal position due to the contribution of a few 5^26^1 sequences.

In samples submitted to more intense heating thermal treatment (1500°C–20 h), well ordered intergrowths are obtained.

- In the samples corresponding to nominal compositions 5^P6^1 long range ordered intergrowths are only observed for $P = 1, 2, 3$. Fig. 6 shows the HRTEM images and SAED patterns obtained along the $[2\bar{1}\bar{1}0]$ and $[1\bar{1}00]$ zone axes for these three microphases. The lack of diffuse streaks along the c^* direction corresponding to the stacking direction attests that

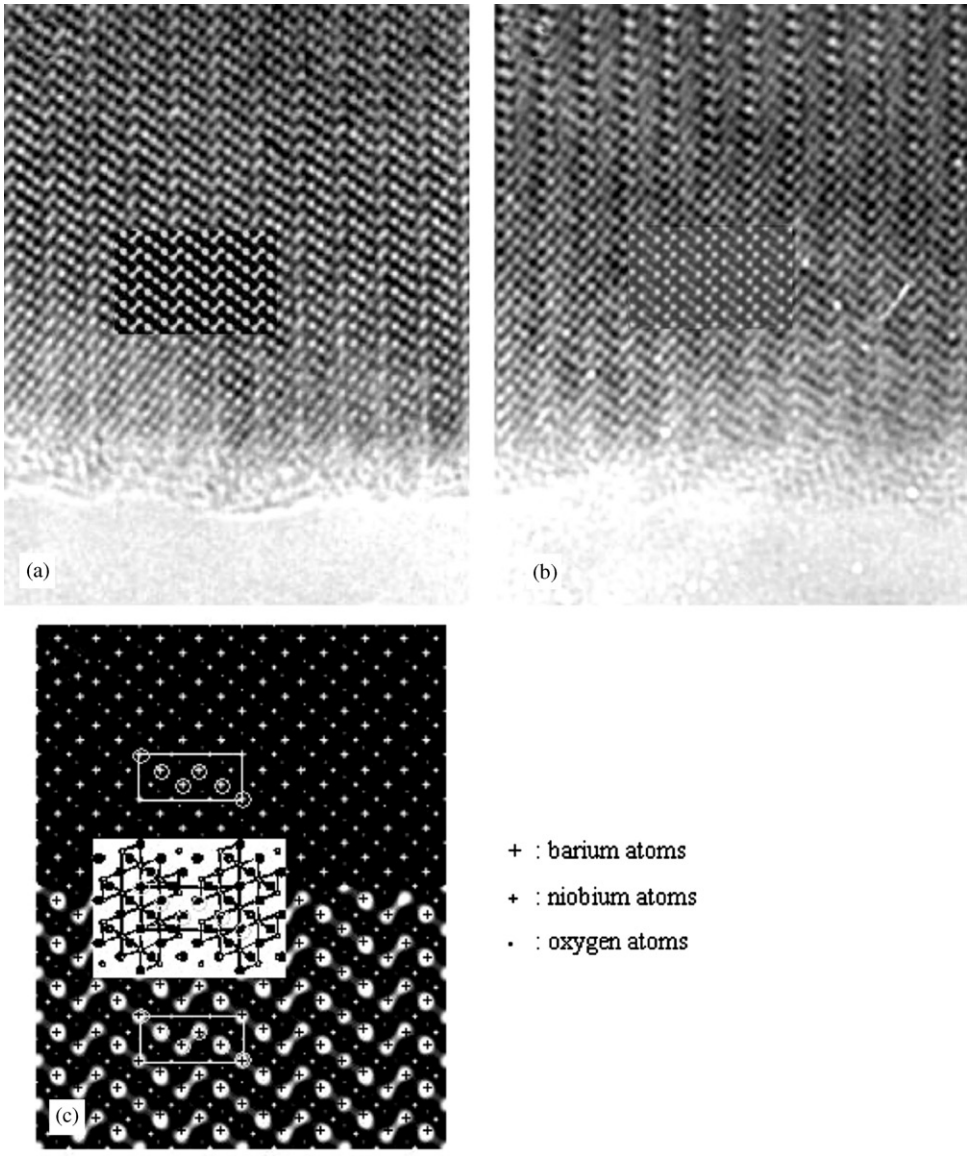

Fig. 4. HRTEM images $Ba_5Nb_4O_{15}$ ($n = 5$) obtained along the $[2\bar{1}\bar{1}0]_H$ zone axis. The simulated image (inserted) corresponds to a defocus value of –45 nm (a) and +33 nm (b) and to a thickness of 19 nm. (c) The correspondence between the simulated image in (a) (lower part) and the projected potential (upper part) shows that white dots represent Ba atoms.

ordered intergrowths are obtained on large crystal domains. For the other nominal compositions with $P > 3$, the expected sequences are only locally observed. Generally, the crystallites display disordered sequences of the most stable microphases previously described (5^16^1, 5^26^1, 5^36^1) together with $n = 5$ single crystals. It is noticeable that the 5^16^1 microphase is particularly stable.

- For the 5^16^Q preparations (Table 1) and even after long annealing treatments, the expected 5^16^Q sequences were never observed. These samples are typically composed of a mixture of (5^P6^1) microphases and ($n = 6$) single crystals.

Moreover, when the composition of the sample is chemically 5^P6^Q, sequences involving two successive blocks of $n = 6$ are never observed. As an example, for the composition $Ba_{43}Ti_3Nb_{32}O_{129}$, chemically, ($5^56^3$) as well as ($5^26^1$)–($5^26^1$)–($5^16^1$) sequences could be expected. It is systematically the latter which are observed (Fig. 7) and complex intergrowths of different 5^P6^1 sequences are always developed.

In this study, we have confirmed that, between $Ba_5Nb_4O_{15}$ ($n = 5$) and $Ba_6TiNb_4O_{18}$ ($n = 6$), intergrowths terms are definitely formed in the $Ba_5Nb_4O_{15}$–$BaTiO_3$ system. Thus, the peak shift observed by Millet et al. [29] in the X-ray diffraction patterns must be

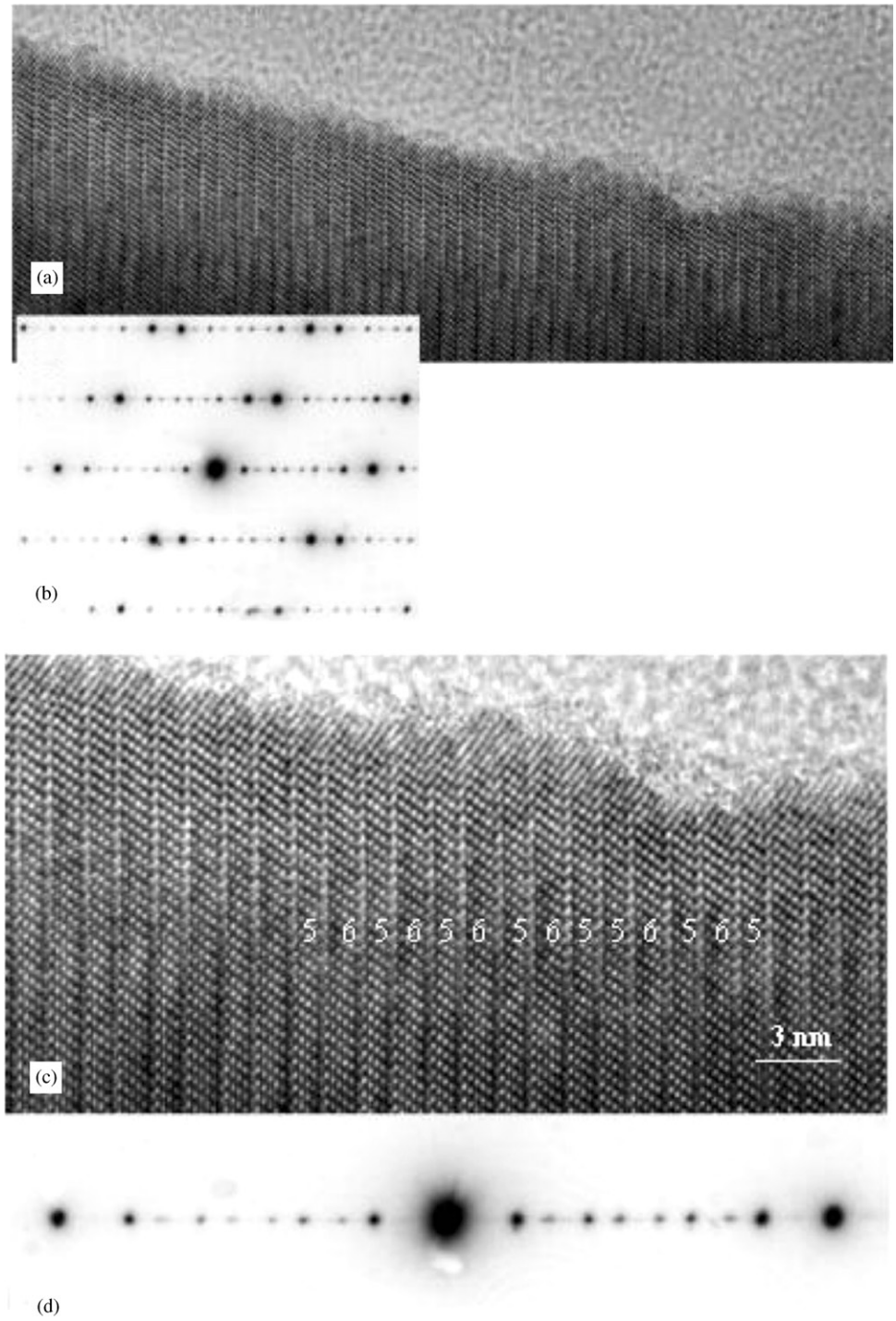

Fig. 5. Observations performed on $Ba_{11}TiNb_8O_{33}$. (a) Overview obtained along the $[2\bar{1}\bar{1}0]_H$ zone axis, (b) selected area diffraction pattern obtained along $[2\bar{1}\bar{1}0]_H$, (c) enlargement showing 5^26^1 stacking faults in the 5^16^1 sequences, (d) the stacking faults result in both diffused strikes and slight displacement of diffraction spots related to the average periodicity of the 5^16^1 sequence.

attributed to the occurrence of a series of microphases based on uniform 5^P6^1 sequences. Even if only a few thermodynamically stable microphases (5^16^1, 5^26^1 and 5^36^1) are obtained in the $Ba_5Nb_4O_{15}$–$BaTiO_3$ system, these results enhance the profound discrepancies with the apparently homologous $La_4Ti_3O_{12}$–$BaTiO_3$ systems. Indeed, as previously indicated, intergrowth terms cannot be formed between $BaLa_4Ti_4O_{15}$ ($n = 5$) and $Ba_2La_4Ti_5O_{18}$ ($n = 6$) and this, whatever the heating treatments [27], resulting in biphasic samples.

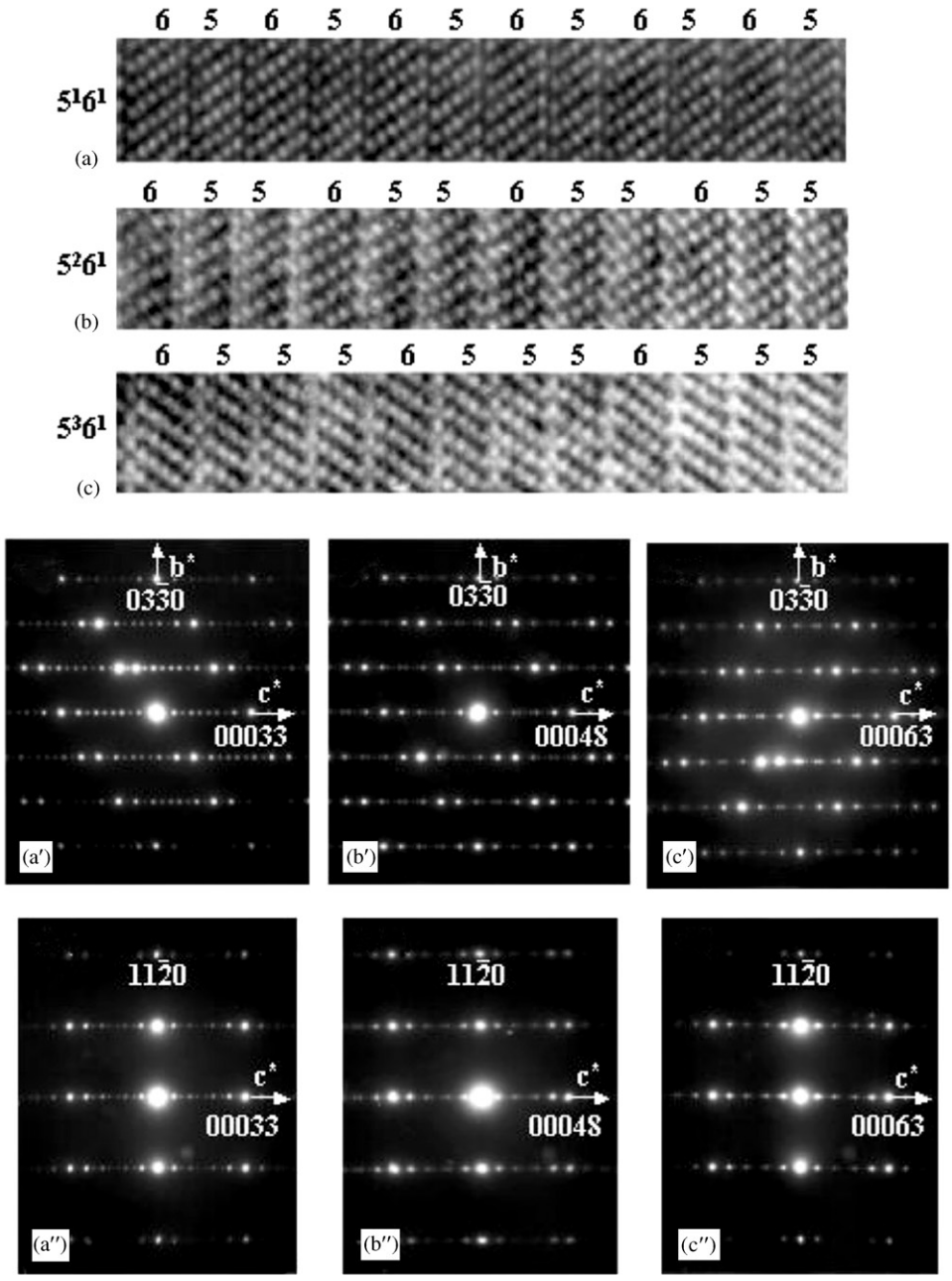

Fig. 6. TEM observations of coherent intergrowth between $Ba_5Nb_4O_{15}$ ($n = 5$) and $Ba_6TiNb_4O_{18}$ ($n = 6$). HRTEM with $[2\bar{1}\bar{1}0]$ zone axis and SAED pattern along both $[2\bar{1}\bar{1}0]$ and $[1\bar{1}00]$ zone axes of 5^16^1 (a, a', a''), 5^26^1 (b, b', b'') and 5^36^1 (c, c', c'').

In order to understand the difference that exists between these two systems we propose to analyze geometrically the anionic sublattices within the AO_3 layers involved in the formation of the interface between two different perovskite-like slabs of $n = 5$ and 6. Indeed, a structural analogy of the AO_3 layers between $n = 5$ and 6 would lead to the formation of an interface where the anionic sublattices would be continuous. Fig. 2a–c and e represent the $[0001]_H$ projections of the AO_3 layers of $n = 5$ and 6 belonging to the two systems. When superimposed, the perfect match between the anionic positions in both layers of $Ba_5Nb_4O_{15}$ and $Ba_6TiNb_4O_{18}$ (Fig. 2c) contrasts with the important mismatch observed in Fig. 2e (superimposition of $BaLa_4Ti_4O_{15}$ and $Ba_2La_4Ti_5O_{18}$ AO_3 layers). We can thus suggest that the geometry of the anionic sublattice plays a key role in the formation of intergrowths. Thus, a discrepancy of 0.35 Å in the anionic positions

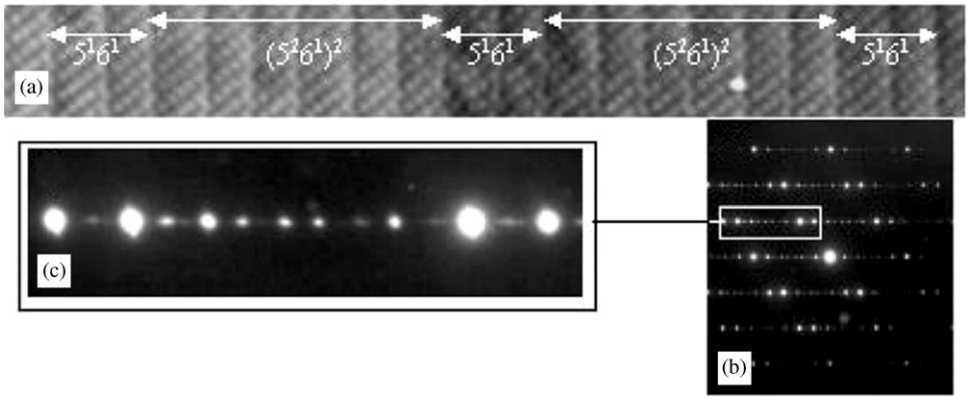

Fig. 7. TEM observation of complex ordered intergrowths between 5^16^1 and 5^26^1.

evidenced in the Fig. 2e impedes the intergrowth formation of 5^P6^1 in the $La_4Ti_3O_{12}$–$BaTiO_3$ system. In such a case the elastic strain involved in the association of the anionic lattices of these two compounds would then be too high. The comparison of these two systems also points out the role of the average size of the A cation through its influence on the geometry of AO_3 layers has been demonstrated in previous papers [13–15]. This phenomenon can be observed in Fig. 2f where the good match between anionic positions in both sublattices (displacements less than 0.1 Å) allows to understand why intergrowths can be developed between $n = 4$ ($La_4Ti_3O_{12}$) and $n = 5$ ($BaLa_4Ti_4O_{15}$) in the $La_4Ti_3O_{12}$–$BaTiO_3$ system [27].

5. Conclusion

This paper shows that in the well-known hexagonal perovskites, the ability to form intergrowths (between $Ba_5Nb_4O_{15}$ and $Ba_6TiNb_4O_{18}$ in the $Ba_5Nb_4O_{15}$–$BaTiO_3$ system) or not (between $BaLa_4Ti_4O_{15}$ and $Ba_2La_4Ti_5O_{18}$ in the $La_4Ti_3O_{12}$–$BaTiO_3$ system), depends on the structural compatibility between the two basic compounds. One of the main criteria that governs the ability to form intergrowths is the accordance of the anionic lattices which is itself dependent on the average size of the A cation.

It results that in a given system of B-cation deficient perovskite, a rough examination of the accurate structure of basic members allows to predict the possibility to form intergrowths. We have also shown that in many cases, the optimization of the annealing treatment led to obtain homogeneous and rather good quality powders of the microphases, which makes possible their structure determination. Thus, the crystal structure of 5^16^1 was determined by X-ray and neutron diffraction analyses [25]. In a forthcoming paper, we will show that the superspace group approach is an optimal tool to describe all these $Ba_n(Ti, Nb)_{n-\delta}O_{3n}$ compounds in a global model.

References

[1] H. Jagodzinski, Acta Crystallogr. 2 (1949) 201.
[2] D. Pandey, P. Krishna, in: T. Hahn (Ed.), International Tables for Crystallography. Vol. C, Kluwer Academic Publishers, Dordrecht, 1989.
[3] C.N.R. Rao, B. Raveau, Transition Metal Oxides, Wiley-VCH, New York, 1998.
[4] J.M. Longo, L. Katz, R. Ward, Inorg. Chem. 4 (2) (1965) 235.
[5] H.J. Von Rother, S. Kemmler-Sack, U. Treiber, W.R. Cyris, Z. Anorg. Allg. Chem. 466 (1980) 131.
[6] F. Galasso, L. Katz, Acta Crystallogr. 14 (1961) 647.
[7] J. Shannon, L. Katz, Acta Crystallogr. B 26 (1970) 102.
[8] R. Bontchev, F. Weill, J. Darriet, Mater. Res. Bull. 27 (1992) 931.
[9] J.R. Carruthers, M. Grasso, J. Electrochem. Soc.: Solid State Sci. 117 (1970) 1426.
[10] N. Teneze, D. Mercurio, G. Trolliard, J.C. Champarnaud, Z. Kristallogr. 215 (2000) 11.
[11] N.F. Fedorov, V.A. Saltykova, M.V. Chistykova, Russ. J. Inorg. Chem. 28 (9) (1980) 2377.
[12] M. German, L.M. Kovba, Russ. J. Inorg. Chem. 30 (2) (1985) 317.
[13] N. Harre, D. Mercurio, G. Trolliard, B. Frit, Mater. Res. Bull. 33 (10) (1998) 1537.
[14] N. Harre, D. Mercurio, G. Trolliard, B. Frit, Eur. J. Solid State Chem. 35 (1998) 77.
[15] N. Teneze, D. Mercurio, G. Trolliard, B. Frit, Mater. Res. Bull. 35 (10) (2000) 1604.
[16] N. Massa, S. Pagola, R. Carbonio, Phys. Rev. B 53 (16) (1996) 8148.
[17] L. Hutchinson, A.J. Jacobson, J. Solid State Chem. 20 (1977) 417.
[18] S. Pagola, G. Polla, G. Leyva, et al., Mater. Sci. Forum 228–231 (1996) 819.
[19] H.C. Van Duivenboden, H.W. Zandbergen, D.J.W. Ijdo, Acta Crystallogr. C 42 (1986) 266.
[20] B. Mossner, S. Kemmler-Sack, J. Less-Common Met. 120 (1986) 287.
[21] R. Bontchev, B. Darriet, J. Darriet, F. Weill, G. Van Tendeloo, S. Amelincks, Eur. J. Solid State Chem. 30 (5) (1993) 521.
[22] G. Van Tendeloo, S. Amelincks, B. Darriet, R. Bontchev, J. Darriet, F. Weill, J. Solid State Chem. 108 (1994) 314.

[23] L. Elcoro, J.M. Perez-Mato, R. Withers, Z. Kristallogr. 215 (2000) 727.
[24] V. Petricek, L. Elcoro, J.M. Perez-Mato, J. Darriet, N. Teneze, D. Mercurio, Ferroelectrics 250 (2001) 31.
[25] N. Teneze, P. Boullay, G. Trolliard, D. Mercurio, Solid State Sci. 4 (2002) 1119.
[26] N. Harre, Ph.D. Thesis, University of Limoges, 1996.
[27] G. Trolliard, N. Harre, D. Mercurio, B. Frit, J. Solid State Chem. 145 (1999) 678.
[28] J.M. Millet, R.S. Roth, L.D. Ettlinger, H.S. Parker, J. Solid State Chem. 67 (1987) 259.
[29] R. Kilaas, Ncemss, Lawrence Berkley Laboratory, University of California, USA, 1996.